Kinetic Analysis of the Reactions of Hypobromous Acid with Protein Components: Implications for Cellular Damage and Use of 3-Bromotyrosine as a Marker of Oxidative Stress†

David I. Pattison* and Michael J. Davies

The Heart Research Institute, 145 Missenden Road, Camperdown, Sydney, NSW 2050, Australia

Received October 30, 2003; Revised Manuscript Received January 21, 2004

ABSTRACT: Hypohalous acids (HOX, X = Cl, Br) are produced by activated neutrophils, monocytes, eosinophils, and possibly macrophages. These oxidants react readily with biological molecules, with amino acids and proteins being major targets. Elevated levels of halogenated Tyr residues have been detected in proteins isolated from patients with atherosclerosis, asthma, and cystic fibrosis, implicating the production of HOX in these diseases. The *quantitative* significance of these findings requires knowledge of the kinetics of reaction of HOX with protein targets, and such data have not been previously available for HOBr. In this study, rate constants for reaction of HOBr with protein components have been determined. The second-order rate constants (22 °C, pH 7.4) for reaction with protein sites vary by 8 orders of magnitude and decrease in the order Cys > Trp ∼ Met ∼ His ∼ α-amino > disulfide > Lys ∼ Tyr ≫ Arg > backbone amides > Gln/Asn. For most residues HOBr reacts 30−100 fold faster than HOCl, though Cys and Met residues are ∼10-fold less reactive, and ring halogenation of Tyr is ∼5000-fold faster. Thus, Tyr residues are more, and Cys and Met much less, important targets for HOBr than HOCl. Kinetic models have been developed to predict the targets of HOX attack on proteins and free amino acids. Overall, these results shed light on the mechanisms of cell damage induced by HOX and indicate, for example, that the 3-chloro-Tyr:3-bromo-Tyr ratio does not reflect the relative roles of HOCl and HOBr in disease processes.

Hypohalous acids (HOX, X = Cl, Br) are strong oxidants with potent antibacterial properties (*1*). HOCl and HOBr are integral factors in mammalian host defense systems and are produced in vivo by activated neutrophils, monocytes, and possibly macrophages (HOCl) and activated eosinophils (HOBr) (*2*, *3*). HOCl and HOBr are formed by the reactions of H_2O_2 with Cl^- or Br^- catalyzed by the heme enzymes, myeloperoxidase (MPO)[1] (*4*) and eosinophil peroxidase (EPO) (*5*). Both HOCl and HOBr react readily with biological molecules including amino acids, proteins, antioxidants (including thiols), carbohydrates, lipids, and DNA (*6*−*14*).

Although HOX formation is crucial for immune response, excessive or misplaced generation can damage host tissues, and this has been implicated in several human inflammatory diseases, including arthritis (*15*), some cancers (*16*−*18*), heart disease (*19*−*21*), cystic fibrosis (*22*), and asthma (*23*−*25*). Elevated levels of EPO and brominated Tyr (Br-Tyr) residues have been detected in the sputum of asthmatic patients relative to controls (*23*−*25*), especially when the patients were subject to an allergen challenge (*24*, *25*). These observations are consistent with a role for EPO and HOBr in asthma.

In light of the potential role of HOX in these diseases, it is important to have a thorough understanding of the chemical modifications induced by these oxidants in biological tissues and, particularly, the reactions that give rise to compounds, such as halogenated Tyr residues, that are used as markers for HOX-mediated damage. To achieve this, a detailed knowledge of the kinetics and products of these reactions is essential. The products of the reactions of HOCl with Cys and Met are disulfides and oxy acids, and sulfoxides, respectively (*9*, *26*, *27*). In the presence of amines it is also possible to generate sulfonamides, via reaction of the initial sulfenyl chloride intermediates with neighboring amine groups (*28*−*30*). Similar reactions are believed to occur with HOBr. The reaction of HOCl with amines (e.g., Lys and α-amino groups) generates unstable chloramine species (RNHCl, RR′NCl) and, when HOCl is in excess, dichloramines ($RNCl_2$) (*31*−*33*). Chloramines on α-amino groups typically decompose within a few minutes of formation to yield aldehydes (*34*), but others such as those on the ϵ-amine group of Lys are more stable, with $t_{1/2}$ >1 h (*35*). HOCl also reacts with amide groups (e.g., protein amide groups) to yield chloramides (*6*, *14*). Analogous processes occur with HOBr (*5*, *12*, *13*), yielding bromamines/amides that are

† This work was funded by Australian Research Council Grants A00001441 and F00001444.

* To whom correspondence should be addressed. Telephone: +61-2-9550-3560. Fax: +61-2-9550-3302. E-mail: d.pattison@hri.org.au.

[1] Abbreviations: apo-A1, apolipoprotein-A1; Br-HPPA, 3-(3-bromo-4-hydroxyphenyl)propionic acid; Br_2-HPPA, 3-(3,5-dibromo-4-hydroxyphenyl)propionic acid; Br-Tyr, 3-bromotyrosine; BSA, bovine serum albumin; $CANH_2$, ϵ-amino-*n*-caproic acid; Cl-Tyr, 3-chlorotyrosine; DTDPA, 3,3′-dithiodipropionic acid; EPO, eosinophil peroxidase; ESI-MS, electrospray ionization mass spectrometry; GSSG, oxidized glutathione; HPLC, high-performance liquid chromatography; HPPA, 3-(4-hydroxyphenyl)propionic acid; HSA, human serum albumin; IAA, 4-imidazoleacetic acid; LDL, low-density lipoprotein; MPO, myeloperoxidase; *N*-acetyl-Br-Tyr, *N*-acetyl-3-bromotyrosine; *N*-acetyl-Br_2-Tyr, *N*-acetyl-3,5-dibromotyrosine.

10.1021/bi035946a CCC: $27.50
Published on Web 03/26/2004

typically more reactive than chloramines/amides (*14*, *36*). The reactions of HOX with Tyr residues generate stable halogenated Tyr residues that are widely used as markers for HOX-mediated damage (*21*, *22*, *24*, *37*−*46*). The major products are 3-chloro- and 3-bromotyrosine (Cl-Tyr and Br-Tyr), but dihalogenated compounds (3,5-dichloro- and 3,5-dibromotyrosine) are formed with high excesses of HOX. The stable products of reaction of HOX with cystine and other amino acid side chains (e.g., His, Trp, and Arg) are poorly characterized for both HOCl and HOBr but probably include 2-oxindole derivatives of Trp and 2-oxohistidine (*33*).

The reaction kinetics for HOCl with biological materials are well established (*6*, *8*−*10*, *32*, *47*−*49*), with the second-order rate constants at pH 7.4 decreasing in the order Met > Cys ≫ cystine ∼ His ∼ α-amino > Trp > Lys ≫ Tyr ∼ Arg > backbone amides > Gln ∼ Asn (*6*). Incorporation of these data into a computational kinetic model has allowed the initial sites of attack of varying molar excesses of HOCl on human serum albumin (HSA), apolipoprotein-A1 (apo-A1), and free amino acids to be predicted; these data correlate well with experimental observations (*6*). Rate constants have also been determined for reaction of HOCl with lipid components and some antioxidants, and these data have been used to model the reactivity of HOCl with lipoproteins and the nucleosome (*7*, *50*).

In contrast to HOCl, there is a paucity of kinetic data for HOBr. It has been reported that the rates of reaction of HOBr with cyclic dipeptides and NADH are ca. 10 times faster than with HOCl (*12*−*14*). Prutz has provided evidence that bromination of the Tyr side chain with HOBr is also more rapid (ca. 250 times) than chlorination by HOCl (*36*) and has intimated that reaction of HOBr with Met side chains is slower than with HOCl (*12*).

In the current work, second-order rate constants have been determined for the reactions of HOBr with model protein substrates at pH 7.4. These data have been incorporated into a computational model to predict the reactivity of HOBr with the plasma protein, HSA, and with plasma concentrations of free amino acids. These predictions have been compared with experimental data and the rate constants compared with those for HOCl. Overall, these show that Br-Tyr is a much more sensitive marker for bromination than Cl-Tyr is for chlorination. This may result in the extent of HOBr-mediated oxidation being overestimated (or HOCl-mediated processes underestimated) on the basis of the yields of Cl-Tyr and Br-Tyr. Furthermore, these data suggest that the more rapid (∼10-fold faster) rate of erythrocyte lysis induced by HOBr compared to HOCl (*51*, *52*) is not due to oxidation or depletion of Cys and Met residues (either low molecular weight or on proteins) and that damage to His, Lys, Tyr, Trp, or cystine residues on proteins could be the key determinant of the rate of cell lysis.

EXPERIMENTAL PROCEDURES

Materials. All chemicals were obtained from Sigma/Aldrich/Fluka and used as received, with the exception of *N*-acetyl-Ala-OMe and cyclo(Asp)$_2$ (Bachem), sodium bromide (>99% purity; Merck), and sodium hypochlorite (in 0.1 M NaOH, low in bromine; BDH Chemicals). The HOCl was standardized by measuring the absorbance at 292 nm at pH 12 [$\epsilon_{292}(^-OCl) = 350\ M^{-1}\ cm^{-1}$] (*53*). All studies were performed in 100 mM phosphate buffer (pH 7.4), except for the HPLC studies which were carried out in 10 mM phosphate buffer (pH 7.4). All phosphate buffers were prepared using Milli Q water and treated with Chelex resin (Bio-Rad) to remove contaminating transition metal ions. The pH values of solutions were adjusted, where necessary, to pH 7.4 using 100 mM H_2SO_4 or 100 mM NaOH.

HOBr Preparation. HOBr was prepared by mixing HOCl (40 mM in H_2O, pH 13) with NaBr (45 mM in H_2O) in equal volumes. The reaction was left for 1 min before dilution with 0.1 M phosphate buffer (pH 7.4) to the required concentration of HOBr (typically 0.2−2.0 mM). As HOBr disproportionates slowly to form Br^- and BrO_2^- (*14*, *36*, *54*), fresh solutions were prepared for each kinetic run and used within 30 min. To investigate whether Br_2 formed in the presence of excess Br^- (*55*) contributed to the observed reaction kinetics, HOBr solutions were also prepared with increasing concentrations of NaBr (45−250 mM). At neutral pH, hypobromous acid exists primarily as HOBr with low concentrations of $^-$OBr also present (pK_a 8.7) (*12*).

Stopped-Flow Studies. Two stopped-flow systems (both 10 mm path length) were used depending on the time scale being studied (*6*). An Applied Photophysics SX.18MV system was used for kinetics on the 10 ms−10 s time scale and a Hi-Tech SFA 20 attachment connected to a PC-controlled Perkin-Elmer Lambda 40 UV/vis spectrometer for reactions on the 5−900 s time scale. For both systems, the sample chamber was maintained at the requisite temperature by circulating water from a thermostated water bath.

Kinetic data were accumulated at 10 nm intervals between 220 and 350 nm (0.1 M phosphate buffer baseline) and combined to give time-dependent spectral data. For the majority of the kinetic experiments (except where stated), HOBr was kept as the limiting reagent, with at least a 2-fold excess of substrate (typically 0.1−1.0 mM HOBr, 0.2−10.0 mM substrate). This reduces the kinetics to pseudo first order and limits the occurrence of secondary reactions (e.g., dibromination). Data were processed by global analysis methods, using Specfit software (version 3.0.15; Spectrum Software Associates; see http://www.bio-logic.fr/rapid-kinetics/specfit.html for further details). All second-order rate constants reported are averages of at least four determinations, and errors are specified as 95% confidence limits.

UV/Vis Spectroscopy. UV/vis spectroscopy was undertaken on a Perkin-Elmer Lambda 40 spectrometer. Spectra were typically acquired (relative to a 0.1 M phosphate buffer baseline) between 220 and 350 nm (1−2 nm intervals), with a time interval of 1−30 min depending on the reaction time scale. The cuvettes were thermostated to 22 °C using a Peltier block. Data were imported into Specfit software and the kinetics processed by global analysis techniques (as above).

HPLC Instrumentation and Methods. Analysis and quantification of *N*-acetyl-Tyr and its reaction products with HOBr were carried out on a Shimadzu LC-10A HPLC system (Shimadzu, South Rydalmere, NSW, Australia). The reaction mixtures were separated on a Zorbax reverse-phase HPLC column (25 cm × 4.6 mm, 5 μM particle size; Rockland Technologies, Newport, DE) packed with octadecyl silanized silica, equipped with a Pelliguard guard column (2 cm; Supelco). The column was maintained at 30 °C using a column oven (Waters Corp., Milford, MA). The mobile phase

was comprised of a gradient of solvent A (10 mM phosphoric acid with 100 mM sodium perchlorate at pH 2.0) and solvent B [80% (v/v) methanol in nanopure H_2O] eluting at 1 mL min^{-1}. The gradient was programmed as follows: 0−5 min, elution with 90% solvent A and 10% solvent B; over the next 5 min the proportion of solvent B was increased to 35%; isocratic elution at 35% solvent B occurred for 35 min; over the following 1 min, solvent B was increased to 50%, and the column was washed at 50% solvent B for 9 min; over the subsequent 5 min the proportion of solvent B was reduced to 10%, and the column was allowed to reequilibrate for 5 min prior to injection of the next sample. The eluent was monitored in series by a UV detector (280 nm), a fluorescence detector (λ_{ex}, 280 nm; λ_{em}, 320 nm), and a dual-channel electrochemical detector (Coulochem II; ESA, Chelmsford, MA). The first channel of the electrochemical detector was set to an oxidation potential of +550 mV (sensitivity, 2 μA) to oxidize any coeluting peaks, and the second channel was set to an oxidation potential of +700 mV (sensitivity, 5 μA) to quantify the halogenated *N*-acetyl-Tyr products. Peak areas were determined using Class VP 6.0 software (Shimadzu) and compared to authentic standards when required. Using these conditions, *N*-acetyl-Tyr was detected in the +700 mV electrochemical channel at a retention time of 14.6 min, *N*-acetyl-3-bromotyrosine (*N*-acetyl-Br-Tyr) at 21.4 min, and *N*-acetyl-3,5-dibromotyrosine (*N*-acetyl-Br_2-Tyr) at 38.0 min. A small impurity peak present in the parent compound was also detected with a retention time of 8.9 min, but this was not characterized further.

The product peaks assigned to *N*-acetyl-Br-Tyr and *N*-acetyl-Br_2-Tyr were characterized by electrospray ionization mass spectrometry (ESI-MS). Approximately 1 mL fractions from eight injections (50 μL) were collected and pooled together. Phosphate and perchlorate salts were removed by reducing the volume of the collected fractions to ca. 65% (to remove MeOH), then loading onto Sep-Pak C18 cartridges (Waters Corp., Milford, MA) that had been preconditioned with MeOH, and equilibrated with solvent A from the HPLC gradient. The cartridges were subsequently washed with nanopure H_2O to elute the water-soluble salts, and the product peaks were then eluted using 100% MeOH. These purified peaks were freeze-dried overnight, and the resulting solid was redissolved in a minimal volume (ca. 200 μL) of 50% aqueous MeOH, containing 1% NH_3 for negative ion ESI-MS.

ESI-MS Characterization of HPLC Product Peaks. The identities of the product peaks from HPLC separation were determined by ESI-MS using a VG Platform mass spectrometer (Fisons, NSW, Australia). The samples were delivered by a syringe pump (Harvard Apparatus 22) with a flow rate of 10 μL min^{-1} with 50 μL of sample used for analysis. A dry N_2 bath gas at atmospheric pressure was employed to assist evaporation of the electrospray droplets. A negative electrospray mode was used with the following settings: capillary potential, 3.0 kV; chicane counter potential, 0.5 V; cone potential, 25 V; gain, 10; acquisition time, 4 min.

The ESI-MS spectrum for the product peak with a retention time of 21.4 min was consistent with *N*-acetyl-Br-Tyr (*m*/*z* 299.8 and 301.8, intensity ratio of 1:1), and that at 38.0 min was consistent with *N*-acetyl-Br_2-Tyr (*m*/*z* 377.7, 379.7, and 381.7, intensity ratio of 1:2:1).

Computational Modeling of HOBr Reactivity. The computational modeling studies of HOBr with HSA and plasma amino acids were performed with Specfit software. A series of individual reactions describing the full reactivity of HSA, or the plasma amino acid composition, were used as the model as described previously for HOCl (*6*). The software was allowed to undergo 100 iterations to yield predicted reactant and product concentrations at time intervals where complete consumption of HOBr had occurred.

RESULTS

Kinetics of HOBr Reaction with Backbone Amide Groups. The kinetics for the reaction of HOBr (1.0 mM) with cyclo$(Gly)_2$ (1.2−4.9 mM; equivalent to 2.4−9.8 mM amide) were investigated at 22 °C. Over 5 s a species with an absorbance band extending from 320 nm into the UV region was formed. The spectral changes are consistent with those observed for the analogous reaction with HOCl (*6*) and are attributed to the formation of cyclo$(Gly)_2$ bromamide. The data were fitted by a simple mechanism [HOBr + cyclo$(Gly)_2$ → bromamide], and Table 1 gives the resulting second-order rate constant. The experiments were repeated at 37 °C, and the second-order rate constant (Table 1) was 3.2 times greater than that at 22 °C. Experiments with HOBr prepared with increasing Br^- excesses gave identical kinetics, suggesting that $HOBr/^-OBr$, and not Br_2, are the major species responsible for the observed reactions. Studies with cyclo$(Ala)_2$, cyclo$(Ser)_2$, and cyclo$(Asp)_2$ yielded similar spectral changes, and the second-order rate constants are shown in Table 1.

Reaction of HOBr (500 μM) with *N*-acetyl-Ala-OMe (2.5−10.0 mM) gave similar spectral changes to the cyclic dipeptides though over a longer time period (6 min). The resulting lower second-order rate constant (Table 1) is consistent with the analogous experiments with HOCl (*6*). A slow decay of the bromamide was observed over a period of 30 min, but the depletion was too small (typically <5%) to obtain an accurate rate constant. Reaction of HOBr (500 μM) with *N*-acetyl-Ala (2.5−50.0 mM) was even slower (60−90 min), and the second-order rate constant for bromamide formation is correspondingly lower (Table 1). The contribution of bromamide decay to the kinetics was much greater than for *N*-acetyl-Ala-OMe, and an approximate first-order decay rate ($k \sim 10^{-4}$ s) was obtained.

Stopped-Flow Kinetics of HOBr Reaction with α-Amino Groups and Amino Acid Side Chains. Reactions of HOBr (100 μM) with α-amino groups were investigated at 22 °C with Gly, Ala, and Val (200−800 μM). Absorbance increases were observed over the full spectral range (220−340 nm) for all substrates with maximal changes at 240 and 290 nm, consistent with the formation of both mono- and dibromamines (*5*). The changes occurred over short time scales (<20 ms) but were readily fitted with a simple mechanism (HOBr + α-amino → product) despite the apparent presence of two products to yield second-order rate constants (Table 1).

The rate of reaction of HOBr with the Lys side chain was investigated with ϵ-amino-*n*-caproic acid ($CANH_2$) and *N*-α-acetyl-Lys. The reaction of HOBr (100 μM) with $CANH_2$ (0.2−2.0 mM) gave a rapid increase in absorbance over the range λ = 230−320 nm, with λ_{max} = 240 nm. These data are consistent with the formation of a mixture of mono- (λ_{max}

Table 1: Second-Order Rate Constants (with 95% Confidence Limits) at 22 °C (Unless Otherwise Stated) and pH 7.2−7.5 (100 mM Phosphate Buffer, except Where Indicated) for Reactions of HOBr with Amino Acid Side Chains, Free α-Amino Groups, and Backbone Amides[a]

Substrate	Structure	Method	k_2 / M^{-1} s^{-1}	Substrate	Structure	Method	k_2 / M^{-1} s^{-1}
Cyclo(Gly)$_2$		Stopped flow	900 ± 100 [a]	2-bromo-4-methylphenol		Stopped flow	$(6.4 \pm 0.3) \times 10^5$
		Stopped flow (37 °C)	$(2.9 \pm 0.3) \times 10^3$ [a]				
Cyclo(Ala)$_2$		Stopped flow	250 ± 30 [a]	3-phenylpropionic acid	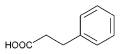	UV/vis	Very slow
Cyclo(Ser)$_2$	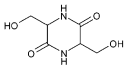	Stopped flow	550 ± 90 [a]	Ethyl guanidine		Stopped flow	$(1.3 \pm 0.2) \times 10^3$
				N-acetyl-Arg-OMe	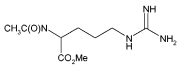	Stopped flow	$(2.2 \pm 0.4) \times 10^3$
Cyclo(Asp)$_2$	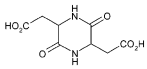	Stopped flow	50 ± 20 [a]	Propionamide		Stopped flow	3.3 ± 0.4
N-acetyl-Ala	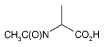	UV/vis	0.07 ± 0.02	2-methyl propionamide		Stopped flow	1.5 ± 0.3
N-acetyl-Ala-OMe	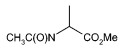	Stopped flow	2.1 ± 0.2	Trimethylacetamide		Stopped flow	0.9 ± 0.1
Gly		Stopped flow	$(2.6 \pm 0.2) \times 10^6$	4-imidazoleacetic acid	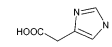	Stopped flow	$\sim 3 \times 10^6$ [c]
Ala		Stopped flow	$(1.6 \pm 0.1) \times 10^6$	3,3'-dithiodipropionic acid		HPLC [d]	$(1.1 \pm 0.2) \times 10^6$
Val		Stopped flow	$(1.7 \pm 0.1) \times 10^6$			HPLC (37 °C) [e]	$(2.3 \pm 0.2) \times 10^6$
ε-aminocaproic acid	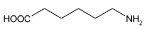	Stopped flow	$(2.6 \pm 0.2) \times 10^5$	(*N*-acetyl-Cys)$_2$	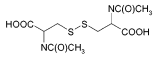	HPLC [d]	$(3.4 \pm 0.8) \times 10^5$
N-α-acetyl-Lys	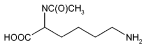	Stopped flow	$(3.6 \pm 0.3) \times 10^5$	*N*-acetyl-Trp	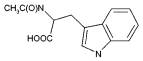	HPLC [d]	$(3.7 \pm 0.3) \times 10^6$
3-(4-hydroxyphenyl) propionic acid	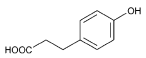	Stopped flow	$(1.6 \pm 0.3) \times 10^5$ [b]	*N*-acetyl-Met-OMe	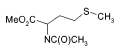	HPLC [d]	$(3.6 \pm 0.3) \times 10^6$
						HPLC (37 °C) [e]	$(9.6 \pm 1.3) \times 10^6$
N-acetyl-Tyr	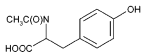	Stopped flow	$(2.6 \pm 0.2) \times 10^5$				
		Stopped flow (37 °C)	$(5.8 \pm 0.2) \times 10^5$				
4-methylphenol		Stopped flow	$(2.6 \pm 0.1) \times 10^5$	*N*-acetyl-Cys	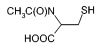	HPLC [d]	$(1.2 \pm 0.2) \times 10^7$

[a] The second-order rate constants are expressed per amide group; therefore, the second-order rates for the substrate are double these values. [b] Second exponential also required for good fits, $k = (3.0 \pm 0.5) \times 10^5$ M^{-1} s^{-1}, consistent with secondary bromination of Br-HPPA. [c] Estimate from competitive stopped-flow studies with *N*-acetyl-Tyr. [d] All reactions undertaken in 10 mM phosphate buffer at 22 °C, and rate constants calculated using eq 5 with $k_{Tyr} = 2.6 \times 10^5$ M^{-1} s^{-1}. [e] All reactions undertaken in 10 mM phosphate buffer at 37 °C, and rate constants calculated using eq 5 with $k_{Tyr} = 5.8 \times 10^5$ M^{-1} s^{-1}.

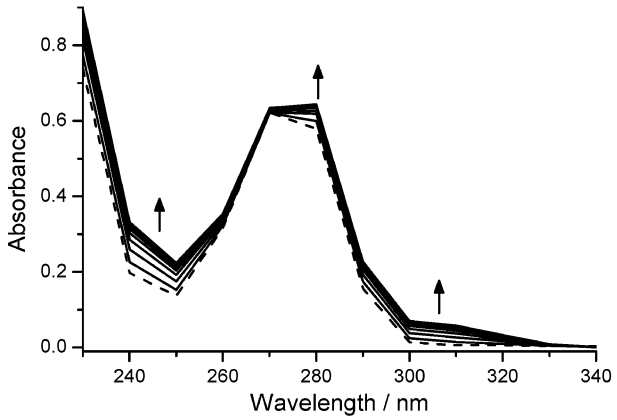

FIGURE 1: Graph of the absorbance changes observed when HOBr (100 μM) was reacted with HPPA (550 μM) at pH 7.4 and 22 °C. The dotted spectrum corresponds to 2 ms after mixing, with subsequent spectra at 5, 10, 15, 20, 25, 30, 35, 40, 45, and 50 ms after mixing.

= 240 nm) and dibromamines (λ_{max} = 290 nm) (*5*). The data were well fitted with a simple mechanism (HOBr + $CANH_2$ → product), and the resulting second-order rate constant is given in Table 1. Experiments with *N*-α-acetyl-Lys gave similar behavior and a comparable second-order rate constant (Table 1).

The reactivity of the Tyr side chain with HOBr was investigated with a variety of compounds. Reaction of HOBr (100 μM) with 3-(4-hydroxyphenyl)propionic acid (HPPA; 280 μM−1.1 mM) resulted in rapid absorbance changes which were complete within 200 ms (Figure 1). The major increases in absorbance occurred at wavelengths on either side (240−250 and 290−320 nm) of the main substrate peak (270 nm), as observed with HOCl (*6*), and are consistent with the formation of 3-bromo-HPPA (Br-HPPA). The data were well fitted by the mechanisms shown in eqs 1 and 2. At lower HPPA:HOBr ratios, dibromination of HPPA (eq 2) became increasingly important. The resulting second-order rate constant for monobrominaton of HPPA is given in Table 1. The reactions were also investigated in the presence of increasing Br^- concentrations (43−250 mM with 40 mM HOCl, i.e., 0.075−6.3-fold molar excess) to investigate the potential role of Br_2 in the observed kinetics. Only minor increases (≤30%) were observed at the highest concentrations of Br^- employed, suggesting that Br_2 does not play a major role in these reactions.

$$\text{HOBr} + \text{HPPA} \xrightarrow{k} \text{Br-HPPA} \quad (1)$$

$$\text{HOBr} + \text{Br-HPPA} \xrightarrow{k} \text{Br}_2\text{-HPPA} \quad (2)$$

N-Acetyl-Tyr and 4-methylphenol were also used as models for the Tyr side chains, and similar data were obtained (Table 1). The second-order rate constant for the reaction of *N*-acetyl-Tyr and HOBr was also determined at 37 °C (Table 1) and was 2.2 times greater than that at 22 °C. The rate of secondary bromination of 3-Br-Tyr by HOBr was investigated (at 22 °C) using 2-bromo-4-methylphenol as a substrate and yielded a second-order rate constant that was ca. 2-fold faster than that for primary bromination of 4-methylphenol (Table 1). This rate constant is consistent with that determined from the analysis of kinetics at low HPPA:HOBr ratios for the process in eq 2. The extent of *N*-acetyl-Br_2-Tyr formation was also assessed by HPLC methods (see below).

Kinetic experiments with 3-phenylpropionic acid (a model for the Phe side chain; 0.25−1.0 mM) did not give any absorbance changes, suggesting that reaction of HOBr with the Phe side chain is very slow. Negative ion ESI-MS studies of the reaction of HOBr with 3-phenylpropionic acid confirmed the absence of products, even after 20 h of reaction.

The reactivity of the Arg side chain was investigated using HOBr (1.0 mM) with ethylguanidine or *N*-acetyl-Arg-OMe (2.5−10 mM). For both substrates, a rapid rise in absorbance (primarily at $\lambda < 270$ nm) was observed within 500 ms of mixing, followed by a decay over a period of 20 s. The data were fitted most accurately using the mechanism shown in eq 3, consistent with comparable reactions with HOCl (*6*). The resulting second-order rate constants are given in Table 1; the first-order decay constant for the intermediate was ca. 0.2 s^{-1}.

$$\text{HOBr} + \text{Arg side chain} \xrightarrow{k_1} \text{intermediate} \xrightarrow{k_2} \text{products} \quad (3)$$

The reactions of HOBr with the amide-containing side chains of Asn and Gln were investigated using propionamide, 2-methylpropionamide, and trimethylacetamide. The reactions of HOBr (0.5 mM) with model amide (2.0−11.0 mM) were monitored either with the SFA 20 stopped-flow attachment or by conventional UV/vis methods, with reaction complete within 5−30 min. All of the reactions resulted in a loss of the OBr^- absorbance (λ, 300−320 nm), with a concomitant increase in absorbance below 280 nm; the data were readily fitted by a simple mechanism (HOBr + amide → product) yielding the second-order rate constants given in Table 1. The resulting spectra are similar to those for chloramides (*6*), consistent with the products being bromamides, RC(O)NHBr. In some cases, there was evidence for subsequent decay of the bromamides over longer time scales; these processes have not been investigated further here.

The reaction of HOBr (1.0 mM) with the His side chain was investigated using 4-imidazoleacetic acid (IAA; 5.0−20 mM) but was too fast to measure directly by stopped-flow methods, even at 10 °C. A new absorbance (<320 nm) appeared within the dead time of the apparatus (~2.5 ms), which subsequently decayed over a period of 100 ms. Similar behavior was observed at lower reactant concentrations (200 μM HOBr, 400 μM−1.5 mM IAA). In an effort to obtain the rate constant by competitive kinetics, experiments were undertaken with 100 μM HOBr and increasing IAA concentrations (200 μM−1.0 mM) in the presence of *N*-acetyl-Tyr (490 μM; 22 °C). Unfortunately, the resulting absorbance changes were insufficient to accurately determine the second-order rate constant, but an estimate of ca. 3×10^6 M^{-1} s^{-1} was obtained. In the presence of IAA the rate of *N*-acetyl-Tyr bromination was inhibited relative to that observed with HOBr alone. This observation is consistent with rapid formation of the IAA bromamine close to, or within, the dead time of the apparatus, followed by subsequent transfer reactions to *N*-acetyl-Tyr. The kinetics and efficiency of these transfer reactions will be reported elsewhere.

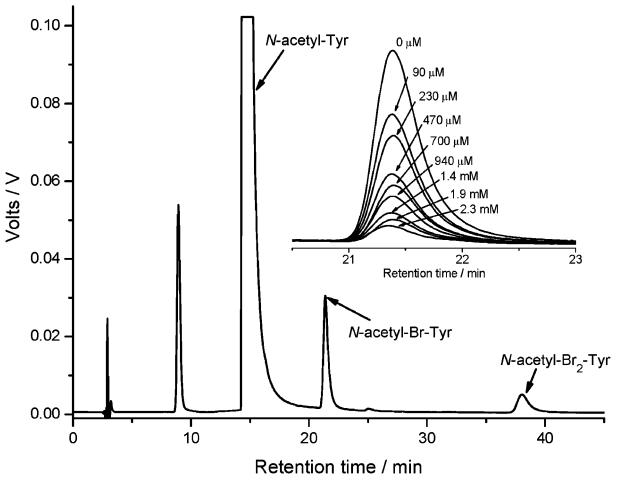

FIGURE 2: HPLC trace showing the formation and separation of *N*-acetyl-Br-Tyr and *N*-acetyl-Br_2-Tyr following incubation of the parent *N*-acetyl-Tyr (900 μM) with HOBr (30 μM). The inset figure shows the depletion of the *N*-acetyl-Br-Tyr peak when the reaction is undertaken in the presence of increasing concentrations of DTDPA (90 μM−2.3 mM).

Competitive Kinetic Studies by HPLC of HOBr Reactions with Amino Acid Side Chains. The reactions of HOBr with Trp, Cys, cystine, and Met side chains were too fast to be measured accurately by direct methods. However, the fast rate of reaction of *N*-acetyl-Tyr with HOBr and the ability to separate brominated *N*-acetyl-Tyr products by HPLC methods (see Experimental Procedures) allowed these rates to be determined by competition kinetics. A similar approach could not be used with the His side chain, as the resulting bromamines also react with the Tyr side chain (*37*, *44*).

The kinetics of the reactions of HOBr (30 μM) with (*N*-acetyl-Cys)$_2$ and another disulfide, 3,3′-dithiodipropionic acid (DTDPA) (both 90 μM−2.3 mM), were investigated in competition with *N*-acetyl-Tyr (900 μM) at 22 °C. The yields of *N*-acetyl-Br-Tyr at each disulfide concentration ($\text{yield}_{\text{quench}}$) were determined by HPLC and compared to the maximal yield in the absence of added quencher ($\text{yield}_{\text{max}}$). A typical HPLC trace and competition plot is shown in Figure 2. Using competition kinetics, the yields of the products of reaction with HOBr are related by eq 4, and rearrangement of this equation results in the linear form given in eq 5. Plots for (*N*-acetyl-Cys)$_2$ and DTDPA are shown in Figure 3a, and the resulting second-order rate constants are given in Table 1.

$$\frac{\text{yield}_{\text{quench}}}{\text{yield}_{\text{max}} - \text{yield}_{\text{quench}}} = \frac{k_{\text{Tyr}}[N\text{-acetyl-Tyr}]}{k_{\text{quench}}[\text{quencher}]} \quad (4)$$

$$\frac{\text{yield}_{\text{max}}[N\text{-acetyl-Tyr}]}{\text{yield}_{\text{quench}}} = \frac{k_{\text{quench}}[\text{quencher}]}{k_{\text{Tyr}}} + [N\text{-acetyl-Tyr}] \quad (5)$$

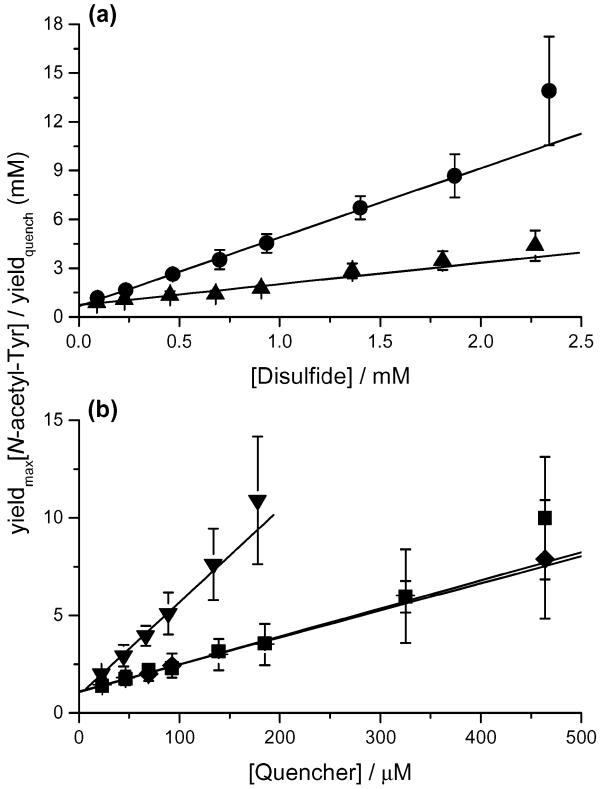

FIGURE 3: Plots of the data and linear analysis for the competitive kinetic data obtained by HPLC methods for the reactions of *N*-acetyl-Tyr with (a) DTDPA (●) and (*N*-acetyl-Cys)$_2$ (▲) and (b) *N*-acetyl-Cys (▼), *N*-acetyl-Met-OMe (◆), and *N*-acetyl-Trp (■). Error bars are representative of 1 SD.

For *N*-acetyl-Cys (20−180 μM), *N*-acetyl-Met-OMe (25−460 μM), and *N*-acetyl-Trp (25−460 μM) a similar approach was used, but with lower HOBr concentrations (10 μM) due to the rapid rates of these reactions. Linear competition plots were obtained in each case (Figure 3b), allowing the second-order rate constants to be determined (Table 1).

The rate constants for reaction of HOBr with DTDPA and *N*-acetyl-Met-OMe were also investigated at 37 °C. The derived second-order rate constants are given in Table 1 and are 2.1 and 2.7 times greater than those at 22 °C, respectively.

It should be noted that eqs 4 and 5 for the competitive kinetic analysis assume that the yield of *N*-acetyl-Br-Tyr is 100% (with respect to added HOBr) in the absence of added quenchers. For these studies, the experimentally determined yields were between 50% and 90%, with the remaining HOBr accounted for by *N*-acetyl-Br$_2$-Tyr formation and other reaction pathways. Thus, the second-order rate constants determined by these methods may underestimate the true second-order rate constants by up to 2-fold, as the calculated second-order rate constant is closely associated with the yield of *N*-acetyl-Br-Tyr in the absence of quencher.

Kinetic Modeling of HOBr Reactivity with HSA. The absolute rate constants determined for HOBr have been incorporated into a computational model (Table 2) to predict the reactivity of HOBr with HSA. The amino acid composition of HSA was obtained from Swissprot (Primary Accession Number P02768), and the extent of reaction of HOBr with each residue was calculated with a range of molar excesses of HOBr (0.17:1 to 170:1). An upper limit for the experimentally observed backbone amide reactivity [$k_2 \sim 10^3$ M^{-1} s^{-1} for cyclo(Gly)$_2$] was used to provide a maximal estimate of direct backbone attack. The results are expressed as the proportion of HOBr reacting at each potential reaction site (Table 3) and as the percentage of each reactive site remaining after reaction (Figure 4a). The former method highlights the residues that are the major sites of HOBr reaction at differing molar excesses, and the latter representation indicates the order and extent to which each residue is depleted with increasing levels of HOBr. These data have been compared (Table 3, Figure 4b) with the analogous HOCl data (*6*), providing insight into the differences between these two oxidants. The predicted ratios of Tyr bromination vs Tyr chlorination have been calculated (Table 4), allowing the significance of experimental halogenated Tyr levels in biological samples to be evaluated.

The modeling results for HSA (Table 3, Figure 4) show that the proportion of HOBr consumed by each residue hardly varies up to a 17-fold molar excess of HOBr, with His residues the major target. Above this excess, the most reactive residues (Met, Cys, His, and Trp) are fully consumed, and an increasing proportion of HOBr reacts at Lys,

Table 2: Parameters Used for Modeling the Reactivity of HOBr with HSA and Free Amino Acids in Plasma[a]

residue	abbreviation	HSA	plasma aa/ μM	k_2(HOBr)/ M^{-1} s^{-1}
His	H	16	89	3.0×10^6
Lys	K	59	167	2.9×10^5
Arg	R	24		1.8×10^3
Asn	N	17		1.9
Gln	Q	20		1.9
Cys	C	1	33	1.2×10^7
Met	M	6	24	3.6×10^6
cystine	SS	17	42	7.2×10^5
Tyr	Y	18	54[b]	2.3×10^5
Trp	W	1	45	3.7×10^6
terminal amine	α	1	2584	2.0×10^6
backbone	BB	583		1.0×10^3

[a] The numbers of reactive side-chain residues and backbone amides present in the protein are given. The second-order rate constants used for the modeling are also shown. The concentrations of free amino acids in plasma were obtained from ref *56*. [b] The rate constants for both the bromination of the aromatic ring and of the α-amino group were included in the model.

Table 3: Results of Computational Modeling for HSA Showing the Percentage of HOX Consumed by Each Potential Reactive Site at Each Molar Excess of HOX over HSA[a]

	molar excess of HOX						
residue	0.17:1	1:1	4:1	8:1	17:1	67:1	170:1
Met	18 (86)	18 (87)	18 (85)	18 (75)	17 (35)	9 (9)	4 (4)
Cys	10 (11)	10 (12)	9 (12)	7 (12)	5 (6)	1 (1)	1 (1)
disulfide	10 (1)	10 (1)	11 (2)	11 (7)	12 (33)	18 (25)	10 (10)
His	40 (1)	40 (1)	40 (1)	40 (4)	39 (21)	24 (24)	10 (10)
Lys	14 (0)	14 (0)	15 (0)	16 (1)	17 (4)	34 (37)	35 (35)
Trp	3 (0)	3 (0)	3 (0)	3 (0)	3 (0)	1 (1)	1 (1)
Tyr	3 (0)	3 (0)	4 (0)	4 (0)	4 (0)	9 (0)	11 (4)
Arg	0 (0)	0 (0)	0 (0)	0 (0)	0 (0)	0 (0)	2 (3)
terminal amine	2 (0)	2 (0)	2 (0)	2 (0)	2 (1)	1 (1)	1 (1)
backbone amide	0 (0)	0 (0)	1 (0)	1 (0)	1 (0)	1 (1)	27 (33)

[a] The results for HOBr are shown, with previous data calculated for HOCl (*6*) given in parentheses. The values for Asn and Gln are not shown, as these were zero at all molar excesses of HOX.

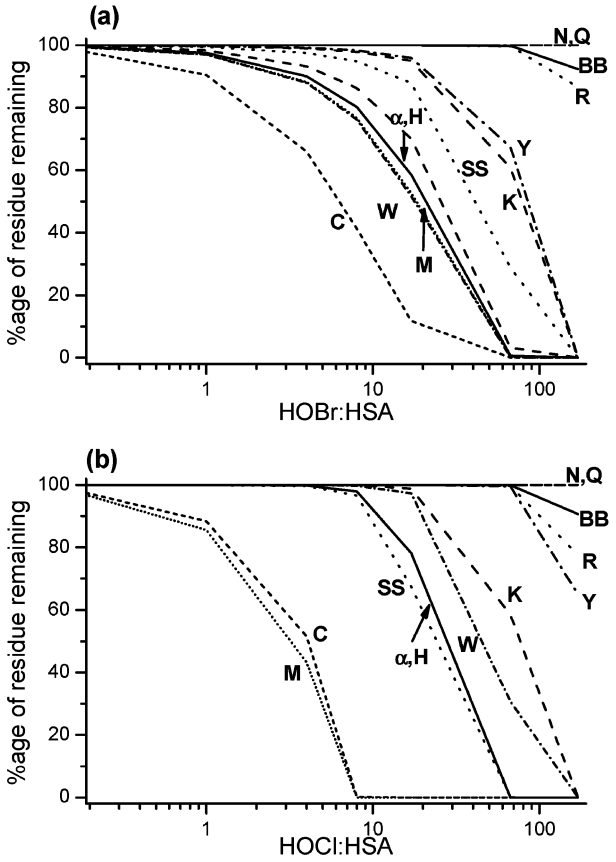

FIGURE 4: Graph showing the predicted percentage of each residue remaining in HSA following reaction with varying molar excesses of (a) HOBr and (b) HOCl (from ref *6*) using the model described in Table 2. Abbreviations are listed in Table 2.

Table 4: Summary of Ratios of Direct Aromatic Bromination vs Chlorination for Tyr Residues in HSA Predicted by Computational Kinetic Modeling

HOX:HSA	Br-Tyr:Cl-Tyr	HOX:HSA	Br-Tyr:Cl-Tyr
0.17	11200	17	370
1	10600	67	70
4	8200	170	3
8	1800		

Tyr, and cystine. At all molar excesses at least 3% of the HOBr is predicted to react with Tyr.

This modeling was repeated with the second-order rate constant (Table 1 for 2-bromo-4-methylphenol) for secondary bromination of the Tyr side chain to yield Br_2-Tyr included. The results (data not shown) predict that <0.5% of the HOBr results in Br_2-Tyr formation at molar excesses up to 17:1 and that Br-Tyr is the predominant Tyr product at these excesses (Br-Tyr:Br_2-Tyr > 15:1). However, with greater molar excesses of HOBr the proportion of Br_2-Tyr formed increases, such that at 67- and 170-fold molar excesses it accounts for approximately 6% and 20% of the HOBr consumed, respectively. At a 67-fold molar excess the predicted Br-Tyr:Br_2-Tyr ratio is 1.5:1, and at 170-fold excess virtually all of the Tyr is converted to Br_2-Tyr.

Kinetic Modeling of HOBr Reactivity with Plasma Amino Acids. Similar modeling has been used to predict the reactivity of HOBr with free amino acids in plasma, using the known concentrations of these species (*56*). For this model (Table 2), the concentration of each reactive side chain has been included, plus the total concentration of free α-amino groups (except for Tyr). For Tyr, rate constants for both the direct bromination of the side chain and attack at the α-amino group have been included in the model to provide information on potential intramolecular transfer reactions from bromamines to the aromatic ring.

Table 5: Results of Computational Modeling for Plasma Amino Acids Showing the Percentage of HOX Consumed by Each Potential Reactive Site at Each Concentration of HOX (20−200 μM)

residue	[HOBr]/μM 20−200[a]	[HOCl]/μM[b] 20	50	75	100	200
Met	1.4	40	36	30	24	12
Cys	6	45	44	40	33	17
disulfide	0.5	0.4	0.5	0.7	1.0	1.7
α-amino	83	14	19	27	40	66
His	4.2	0.5	0.6	0.9	1.4	2.3
Lys	0.8	0	0.1	0.1	0.1	0.2
Trp	2.6	0	0	0.1	0.1	0.1
Tyr (ring)	0.2	0	0	0	0	0
Tyr (α-amino)	1.7	0.3	0.4	0.6	0.8	1.4

[a] The percentages of HOBr consumed by each residue were independent of concentration; thus the results are summarized as a single column. [b] HOCl results are taken from ref *6*.

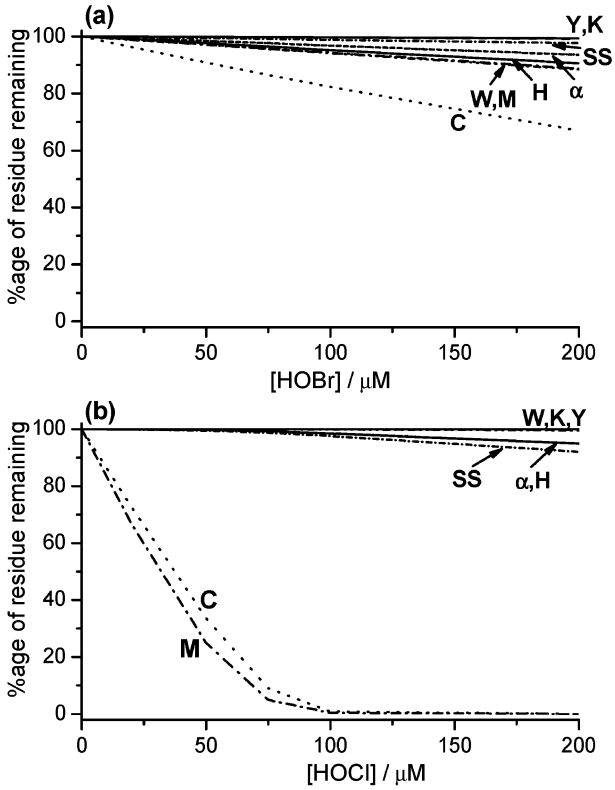

FIGURE 5: Graph showing the predicted percentage of each reactive site remaining in free amino acids in plasma following reaction with varying molar excesses of (a) HOBr and (b) HOCl (from ref *6*) using the model described in Table 2. Abbreviations are listed in Table 2.

The modeling predicts that for HOBr concentrations up to 200 μM the major target is the free α-amino groups (ca. 80%; Table 5). At, or below, this concentration there is virtually no variation in the pattern of reactivity for HOBr. Interestingly, it is predicted that ca. 2% of the HOBr reacts with Tyr and that the ratio of α-amino vs ring attack is approximately 9:1. Thus, despite the rapid rate of direct ring

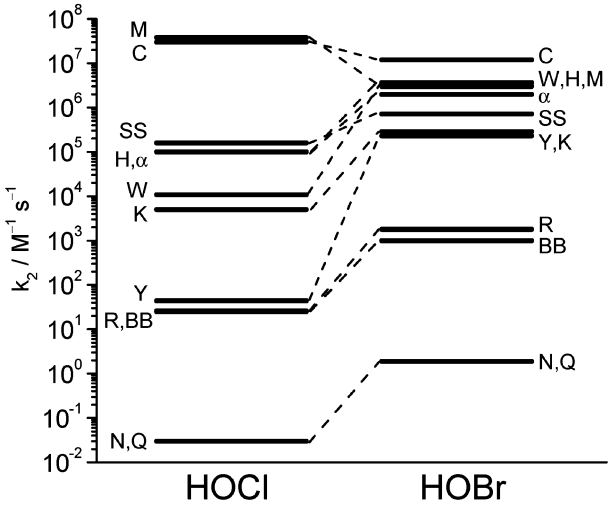

FIGURE 6: Schematic diagram summarizing the second-order rate constants for the reactions of HOBr and HOCl (from ref *6*) with various protein components. The value for backbone amides (BB) represents that for cyclo(Gly)$_2$ and is regarded as a maximal estimate of the rate that occurs in proteins. Abbreviations are listed in Table 2.

halogenation the major site of reaction with free Tyr is the α-amino group. The modeling data also predict that there is no selective depletion of particular species (Figure 5a), which is in stark contrast to HOCl (Figure 5b) (*6*).

DISCUSSION

The second-order rate constants for the reactions of HOBr with protein components are summarized schematically in Figure 6 and are compared to the HOCl data reported previously (*6*). There is a general increase in rate of ca. 30-fold for HOBr over HOCl, but there are some noticeable deviations which warrant discussion.

Wajon and Morris have previously investigated the kinetics of HOBr with ammonia, Gly, and glutamate (*13*). At pH 7.1, they determined that $k_2 \sim 3.5 \times 10^5$ M^{-1} s^{-1} for reaction of HOBr with ammonia, and extrapolation of data obtained at pH 10−12 for Gly yielded $k_2 \sim 4.6 \times 10^5$ M^{-1} s^{-1} at pH 7.0. These values are in reasonable agreement with the rates determined here for α-amino groups at pH 7.4, particularly considering that the maximal observed second-order rate constant is predicted to occur at the average of the pK_a values for HOBr and the substrate (for Gly this is at pH 9.3) (*13*). This group reported that bromination of amines is 3−15 times faster than chlorination (*13*); the current study suggests that for α-amino groups the increase is somewhat greater (up to 20-fold).

Bromination of monobromamines to form dibromamines is facile, and transfer reactions (equilibration processes) between free amines and mono- and dibromamines occur more readily than with the analogous chloramines (*13*). Studies with taurine have shown that dibromamine formation occurs readily when the amine is present at <200-fold excesses (*5*). These observations are consistent with the results presented here, where the final absorbance spectra following reaction of α-amino groups with HOBr contain both mono- and dibromamines. However, the kinetic analysis did not reveal the presence of more than one process, and it is proposed that the equilibration process occurs extremely rapidly at neutral pH.

Similar spectral data were observed for the Lys side chain, and rapid equilibration probably occurs with these substrates too. This residue shows an almost 60-fold increase in the rate of bromination vs chlorination, making it a relatively more important target than the α-amino group for HOBr than HOCl (*6*).

The reaction of HOBr with cyclo(Gly)$_2$ has been reported to occur with $k_2 = 1.2 \times 10^3$ M^{-1} s^{-1} (pH 7.2, 20 °C) (*14*). A value of $k_2 = 1.9 \times 10^3$ M^{-1} s^{-1} at pH 7.4 can be calculated from the provided data (*14*), which is close to the value of $(1.8 \pm 0.2) \times 10^3$ M^{-1} s^{-1} reported here. Prutz's data indicate that there is a 20-fold increase in rate of halogenation of the amide group of cyclo(Gly)$_2$ on switching from HOCl to HOBr (*14*). Our studies suggest the difference in rate constants is consistently larger (ca. 30-fold) with a wide range of backbone amides (*6*); with side-chain amides (Asn and Gln) this rate enhancement is even larger (40−100-fold) (*6*). Interestingly, the second-order rate constants for reactions of HOBr with the various peptide amides vary by 4 orders of magnitude. Similar variation was observed with HOCl and is attributed to a combination of conformational (cyclic vs linear) and charge (neutral vs charged) effects (*6*).

Few studies have been carried out previously with the sulfur-containing residues (Cys, Met, cystine). Prutz et al. have utilized oxidized glutathione (GSSG) and Met to inhibit the oxidation of NADH by HOBr (*12*), and their data for GSSG show that only 20% of the oxidant reacts at the disulfide group with the remainder reacting with the α-amino function. Using this percentage and the value of $k_2 = 2 \times 10^6$ M^{-1} s^{-1} for the α-amino groups in Table 1, an estimate of $k_2 \sim 1 \times 10^6$ M^{-1} s^{-1} for reaction with the disulfide group can be obtained. This is in good agreement with the value for k_2 determined for DTDPA (Table 1), but with the more sterically hindered and more relevant model for cystine residues in proteins (*N*-acetyl-Cys)$_2$, k_2 is reduced almost 3-fold. The values reported here are consistent with previous suggestions (*12*). Interestingly, the rate constant for DTDPA with HOBr is only 7 times faster than that for HOCl (*6*), which is in contrast to other residues where the rate is typically >20 times faster.

An approximate second-order rate constant was calculated for the reaction of HOBr with Met, $k_2 \sim 4 \times 10^6$ M^{-1} s^{-1} from competition with NADH (*12*). This is almost identical to the value determined here. These data are particularly noteworthy as it is >10 times *lower* than that for HOCl (*6*, *32*). Reaction of HOBr with the Cys side chain is also slower (ca. 2.5-fold) than with HOCl (*6*, *32*). These lower rate constants are consistent with these residues being much less important targets for HOBr, when compared to HOCl, and these residues are therefore unlikely to act as "sacrificial antioxidants" in protein oxidation by HOBr, as suggested for HOCl-mediated protein damage (*57*−*59*).

In contrast to the above, where HOBr reacts more slowly than HOCl, halogenation of Tyr side chains was found to occur ca. 5000 times faster with HOBr (*6*). A less dramatic increase in rate has been reported previously (*36*) with cyclo(Ser-Tyr) at pH 7.8 ($k_2 \sim 1.2 \times 10^5$ M^{-1} s^{-1} and 490 M^{-1} s^{-1} for HOBr and HOCl, respectively, i.e., ca. 250-fold). The value for HOBr is similar to that reported here, but the HOCl rate is higher than that determined previously (*6*). The ca. 5000-fold larger values reported here are con-

sistent with data for the model compound 4-methylphenol [k_2(HOCl) $\sim$ 50 M^{-1} s^{-1} and k_2(HOBr) $\sim$ 3 $\times$ 10^5 M^{-1} s^{-1}] (*60*, *61*). A role for Br_2 in this bromination was discounted due to the low level of Br_2 present in solution (*61*), and this is consistent with the detection of only minor increases in k_2 in the current study when HOBr was prepared in the presence of large excesses of Br^-. The consistent and dramatic increases in the rate of halogenation of phenols by HOBr over HOCl have important implications for studies of protein oxidation and, particularly, the use of halogenated Tyr residues as markers of HOX-mediated damage (see below).

Computational modeling has been used previously to predict and reconcile data for HOCl-mediated oxidation of proteins and lipoproteins (*6*, *7*). The potential limitations of this modeling have been discussed (*6*, *7*), and these also apply here. In particular, two major factors cannot be incorporated readily: (a) differing accessibility to the various residues present in a protein and (b) variations in pK_a (and hence reactivity) for some residues (e.g., Cys, His) due to their environment. It is known that the reactions between HOCl and amines, His, Met, and Cys side chains are all sensitive to pH (*6*, *32*, *47*). For amines and His, the greatest rate constant occurs at the pH corresponding to the average of the pK_a's for HOCl and the substrate; the relationships for Met and Cys are more complex. Similar pH dependences are likely to apply for HOBr, but these have not been investigated in detail. A further concern is that the order of reactivity differs at 37 °C when compared to 22 °C, due to differences in activation energy for the reactions. The second-order rate constants for selected residues [cyclo(Gly)$_2$, *N*-acetyl-Tyr, DTDPA, and *N*-acetyl-Met-OMe] have been determined at both 22 and 37 °C, and in each case the rate constant is between 2.1- and 3.2-fold greater at 37 °C than at 22 °C. These compounds have markedly different structures; thus the close similarities in rate increase provide evidence that the order of reactivity with HOBr at 37 °C is not dramatically different from that at 22 °C.

Despite these limitations, there is good agreement between predicted and experimental data for HOCl (*6*, *7*), giving confidence that predictions for HOBr are also valid. Preliminary studies with lysozyme show good correlation between the destruction of Trp by increasing molar excesses of HOCl or HOBr and the Trp consumption predicted by these computational models (C. L. Hawkins, D. I. Pattison, and M. J. Davies, unpublished data). Unfortunately, there are too few detailed studies of HOBr-mediated protein oxidation to allow further direct confirmation of the predicted data. Low levels of Br-Tyr have been detected on bovine serum albumin (BSA) following incubation with MPO in the presence of plasma levels of Cl^- and Br^-, but the levels of Cl-Tyr were not quantified (*37*). Analysis of BSA exposed to activated neutrophils in Hank's balanced salt solution (140 mM Cl^-) supplemented with 100 μM Br^- (ca. physiological plasma levels) (*62*) revealed that Cl-Tyr levels were ca. 6 times higher than Br-Tyr levels (*24*), but the concentrations of HOCl and HOBr generated were not determined. A study of low-density lipoprotein (LDL) oxidation has shown that Trp and cystine residues of apolipoprotein-B are depleted more, and Lys residues less, readily by HOBr than HOCl (*63*). Although LDL oxidation cannot be modeled directly with the current information, the HSA data predict greater Trp consumption by HOBr than HOCl and little difference in Lys and cystine consumption; the last observation is at odds with the LDL studies (*63*), but this model does not include secondary reactions which may give rise to this difference.

Halogenated Tyr residues are commonly used to quantify HOX-mediated damage in diseased tissues (*21*−*25*, *37*−*46*), and the formation of Br-Tyr is increasingly being used as evidence for EPO-mediated damage (*23*−*25*, *44*). The data presented here show that care needs to be taken when using the abundance of Cl-Tyr and Br-Tyr to assess the relative importance of HOBr and HOCl, as Br-Tyr is formed much more readily, and to a greater extent, than Cl-Tyr for any given concentration of HOX. This is particularly true for the low molar excesses of oxidant likely to be present physiologically. This may result in an overestimation of the importance of HOBr (or an underestimation of the importance of HOCl) in cases where both species may be formed. This is clearly illustrated by the prediction that the amount of Br-Tyr generated on HSA at a 0.17:1 molar excess of HOBr:HSA is ca. 3 times greater than the amount of Cl-Tyr generated with a 100-fold greater molar excess of HOCl (17:1).

The levels of protein-bound Br-Tyr and Cl-Tyr in bronchoalveolar lavage fluid from patients with asthma have been investigated (*24*). A 35-fold increase in Br-Tyr and ca. 3-fold elevation in Cl-Tyr levels were observed 48 h after allergen challenge in asthmatics but not in controls. The eosinophil count remained constant for the nonasthmatic controls but increased more than 150-fold in the asthmatic patients, while the neutrophil levels increased ca. 7-fold for both asthmatic and nonasthmatic patients (*24*). These results indicate that HOBr is the major oxidant present in this system. Similar data were reported in a further study (*25*), but the neutrophil counts were not reported. These authors suggested that the ratio of Br-Tyr:Cl-Tyr could be used to indicate a preferential contribution of eosinophils to the observed damage. The data presented here show that this is not necessarily true and that to confirm this hypothesis the levels of neutrophils and eosinophils, and preferably the activities of MPO and EPO, need to be assessed directly (cf. the more complete data in ref *23*).

The computational studies for free amino acids in plasma suggest that the major target for HOBr is the α-amino group to yield bromamines, whereas HOCl targets the sulfur-containing amino acids (*6*). Low HOBr concentrations also directly brominate the Tyr side chain, whereas no halogenation is predicted even with high HOCl concentrations. Even higher Br-Tyr levels than those predicted by this model may occur as a result of secondary Tyr bromination induced by initial bromamines [cf. data for taurine and *N*-α-acetyl-Lys (*37*, *44*)].

The levels of halogenated Tyr have been investigated in a mouse model of sepsis (*44*). Twenty-four hours after the induction of sepsis, peritoneal lavage was carried out, and the extracted free amino acids were analyzed. Cl-Tyr levels were increased 16-fold, and Br-Tyr 6-fold, relative to controls. The peroxidase activity in the lavage fluid was shown to be due primarily to MPO. Similar experiments with MPO-deficient mice revealed no increase in Cl-Tyr but a 2.5-fold increase in Br-Tyr, suggesting that MPO generates both chlorinating and brominating oxidants in vivo (*44*).

Studies on the specificity of MPO for Cl^-, Br^-, and SCN^- have shown that HOBr production at physiological ion concentrations accounts for less than 5% of the H_2O_2 consumed by MPO (*62*). In light of the current data (Figure 5, Table 5), a 95:5 HOCl:HOBr ratio would yield detectable levels of Br-Tyr with the free amino acid, and hence it is not surprising that Br-Tyr was observed in the sepsis model where only neutrophils, and thus MPO, are present (*44*).

The data presented here also provide potential insights into the mechanisms of cell lysis induced by HOX and, particularly, the observation that HOBr effects lysis of erythrocytes ca. 10 times more efficiently than HOCl (*51*, *52*). This is unlikely to be due to the rate of cell penetration by these oxidants, as the effect is specific to erythrocytes, with no difference in cell lysis rate observed for macrophages (J774 or THP1 cells) (*52*). The current data suggest that this difference is unlikely to be due to depletion of GSH or protein thiols, or oxidation of Met residues, as HOCl reacts more rapidly with these targets than HOBr; this is consistent with experimental observations (*64*−*66*). It has been postulated that modification of membrane proteins is a key factor with irreversible cross-linking occurring more readily with HOBr (*51*). The results presented here suggest that His, Lys, Trp, and Tyr (and possibly cystine) side chains, but not Cys or Met, are the most crucial targets on such proteins, as HOBr reacts more readily with these species than HOCl at low oxidant levels.

ACKNOWLEDGMENT

The authors thank Prof. Peter Lay and Dr. Aviva Levina (University of Sydney) for the use of the Applied Photophysics SX.18MV stopped-flow system and Dr. Clare Hawkins (The Heart Research Institute) for helpful discussions.

REFERENCES

1. Thomas, E. L. (1979) Myeloperoxidase, hydrogen peroxide, chloride antimicrobial system: Nitrogen−chlorine derivatives of bacterial components in bactericidal action against *Escherichia coli*, *Infect. Immun. 23*, 522−531.
2. Zgliczynski, J. M., Stelmaszynska, T., Ostrowski, W., Naskalski, J., and Sznajd, J. (1968) Myeloperoxidase of human leukaemic leucocytes. Oxidation of amino acids in the presence of hydrogen peroxide, *Eur. J. Biochem. 4*, 540−547.
3. Weiss, S. J., Test, S. T., Eckmann, C. M., Roos, D., and Recvani, S. (1986) Brominating oxidants generated by human eosinophils, *Science 234*, 200−203.
4. Klebanoff, S. J. (1999) Myeloperoxidase, *Proc. Assoc. Am. Phys. 111*, 383−389.
5. Thomas, E. L., Bozeman, P. M., Jefferson, M. M., and King, C. C. (1995) Oxidation of bromide by the human leukocyte enzymes myeloperoxidase and eosinophil peroxidase. Formation of bromamines, *J. Biol. Chem. 270*, 2906−2913.
6. Pattison, D. I., and Davies, M. J. (2001) Absolute rate constants for the reaction of hypochlorous acid with protein side-chains and peptide bonds, *Chem. Res. Toxicol. 14*, 1453−1464.
7. Pattison, D. I., Hawkins, C. L., and Davies, M. J. (2003) Hypochlorous acid mediated oxidation of lipid components and antioxidants present in low-density lipoproteins: Absolute rate constants, product analysis and computational modeling, *Chem. Res. Toxicol. 16*, 439−449.
8. Winterbourn, C. C. (1985) Comparative reactivities of various biological compounds with myeloperoxidase-hydrogen peroxide-chloride, and similarity of the oxidant to hypochlorite, *Biochim. Biophys. Acta 840*, 204−210.
9. Folkes, L. K., Candeias, L. P., and Wardman, P. (1995) Kinetics and mechanisms of hypochlorous acid reactions, *Arch. Biochem. Biophys. 323*, 120−126.
10. Prutz, W. A. (1996) Hypochlorous acid interactions with thiols, nucleotides, DNA, and other biological substrates, *Arch. Biochem. Biophys. 332*, 110−120.
11. Hawkins, C. L., and Davies, M. J. (1998) Degradation of hyaluronic acid, poly- and monosaccharides, and model compounds by hypochlorite: Evidence for radical intermediates and fragmentation, *Free Radical Biol. Med. 24*, 1396−1410.
12. Prutz, W. A., Kissner, R., Koppenol, W. H., and Ruegger, H. (2000) On the irreversible destruction of reduced nicotinamide nucleotides by hypohalous acids, *Arch. Biochem. Biophys. 380*, 181−191.
13. Wajon, J. E., and Morris, J. C. (1982) Rates of formation of *N*-bromo amines in aqueous solution, *Inorg. Chem. 21*, 4258−4263.
14. Prutz, W. A. (1999) Consecutive halogen transfer between various functional groups induced by reaction of hypohalous acids: NADH oxidation by halogenated amide groups, *Arch. Biochem. Biophys. 371*, 107−114.
15. Davies, J. M., Horwitz, D. A., and Davies, K. J. (1993) Potential roles of hypochlorous acid and *N*-chloroamines in collagen breakdown by phagocytic cells in synovitis, *Free Radical Biol. Med. 15*, 637−643.
16. Jesaitis, A. J., and Dratz, E. A. (1992) *The molecular basis of oxidative damage by leukocytes*, pp 1−368, CRC Press, Boca Raton, FL.
17. Weitzman, S. A., and Gordon, L. I. (1990) Inflammation and cancer: Role of phagocyte-generated oxidants in carcinogenesis, *Blood 76*, 655−663.
18. Ohshima, H., Tatemichi, M., and Sawa, T. (2003) Chemical basis of inflammation-induced carcinogenesis, *Arch. Biochem. Biophys. 417*, 3−11.
19. Zhang, R., Brennan, M. L., Fu, X., Aviles, R. J., Pearce, G. L., Penn, M. S., Topol, E. J., Sprecher, D. L., and Hazen, S. L. (2001) Association between myeloperoxidase levels and risk of coronary artery disease, *J. Am. Med. Assoc. 286*, 2136−2142.
20. Hazell, L. J., Arnold, L., Flowers, D., Waeg, G., Malle, E., and Stocker, R. (1996) Presence of hypochlorite-modified proteins in human atherosclerotic lesions, *J. Clin. Invest. 97*, 1535−1544.
21. Hazen, S. L., and Heinecke, J. W. (1997) 3-Chlorotyrosine, a specific marker of myeloperoxidase-catalysed oxidation, is markedly elevated in low-density lipoprotein isolated from human atherosclerotic intima, *J. Clin. Invest. 99*, 2075−2081.
22. van der Vliet, A., Nguyen, M. N., Shigenaga, M. K., Eiserich, J. P., Marelich, G. P., and Cross, C. E. (2000) Myeloperoxidase and protein oxidation in cystic fibrosis, *Am. J. Physiol. Lung Cell Mol. Physiol. 279*, L537−L546.
23. Aldridge, R. E., Chan, T., Van Dalen, C. J., Senthilmohan, R., Winn, M., Venge, P., Town, G. I., and Kettle, A. J. (2002) Eosinophil peroxidase produces hypobromous acid in the airways of stable asthmatics, *Free Radical Biol. Med. 33*, 847−856.
24. Wu, W., Samoszuk, M. K., Comhair, S. A., Thomassen, M. J., Farver, C. F., Dweik, R. A., Kavuru, M. S., Erzurum, S. C., and Hazen, S. L. (2000) Eosinophils generate brominating oxidants in allergen-induced asthma, *J. Clin. Invest. 105*, 1455−1463.
25. MacPherson, J. C., Comhair, S. A. A., Erzurum, S. C., Klein, D. F., Lipscomb, M. F., Kavuru, M. S., Samoszuk, M. K., and Hazen, S. L. (2001) Eosinophils are a major source of nitric oxide-derived oxidants in severe asthma: Characterization of pathways available to eosinophils for generating reactive nitrogen species, *J. Immunol. 166*, 5763−5772.
26. Pereira, W. E., Hoyano, Y., Summons, R. E., Bacon, V. A., and Duffield, A. M. (1973) Chlorination studies. II. The reaction of aqueous hypochlorous acid with α-amino acids and dipeptides, *Biochim. Biophys. Acta 313*, 170−180.
27. Silverstein, R. M., and Hager, L. P. (1974) The chloroperoxidase-catalyzed oxidation of thiols and disulfides to sulfenyl chlorides, *Biochemistry 13*, 5069−5073.
28. Fu, X., Mueller, D. M., and Heinecke, J. W. (2002) Generation of intramolecular and intermolecular sulfenamides, sulfinamides, and sulfonamides by hypochlorous acid: A potential pathway for oxidative cross-linking of low-density lipoprotein by myeloperoxidase, *Biochemistry 41*, 1293−1301.
29. Raftery, M. J., Yang, Z., Valenzuela, S. M., and Geczy, C. L. (2001) Novel intra- and intermolecular sulfinamide bonds in S100A8 produced by hypochlorite oxidation, *J. Biol. Chem. 276*, 33393−33401.
30. Pullar, J. M., Vissers, M. C., and Winterbourn, C. C. (2001) Glutathione oxidation by hypochlorous acid in endothelial cells

produces glutathione sulfonamide as a major product but not glutathione disulfide, *J. Biol. Chem. 276*, 22120−22125.
31. Thomas, E. L., Grisham, M. B., and Jefferson, M. M. (1986) Preparation and characterization of chloramines, *Methods Enzymol. 132*, 569−585.
32. Armesto, X. L., Canle, M., Fernandez, M. I., Garcia, M. V., and Santaballa, J. A. (2000) First steps in the oxidation of sulfur-containing amino acids by hypohalogenation: Very fast generation of intermediate sulfenyl halides and halosulfonium cations, *Tetrahedron 56*, 1103−1109.
33. Hawkins, C. L., Pattison, D. I., and Davies, M. J. (2003) Hypochlorite-induced oxidation of amino acids, peptides and proteins, *Amino Acids 25*, 259−274.
34. Hazen, S. L., d'Avignon, A., Anderson, M. A., Hsu, F. F., and Heinecke, J. W. (1998) Human neutrophils employ the myeloperoxidase-hydrogen peroxide-chloride system to oxidise α-amino acids to a family of reactive aldehydes, *J. Biol. Chem. 273*, 4997−5005.
35. Hawkins, C. L., and Davies, M. J. (1998) Reaction of HOCl with amino acids and peptides: EPR evidence for rapid rearrangement and fragmentation reactions of nitrogen-centered radicals, *J. Chem. Soc., Perkin Trans. 2*, 1937−1945.
36. Prutz, W. A., Kissner, R., Nauser, T., and Koppenol, W. H. (2001) On the oxidation of cytochrome *c* by hypohalous acids, *Arch. Biochem. Biophys. 389*, 110−122.
37. Wu, W. J., Chen, Y. H., d'Avignon, A., and Hazen, S. L. (1999) 3-bromotyrosine and 3,5-dibromotyrosine are major products of protein oxidation by eosinophil peroxidase: Potential markers for eosinophil-dependent tissue injury in vivo, *Biochemistry 38*, 3538−3548.
38. Kettle, A. J. (1996) Neutrophils convert tyrosyl residues in albumin to chlorotyrosine, *FEBS Lett. 379*, 103−106.
39. Hazen, S. L., Crowley, J. R., Mueller, D. M., and Heinecke, J. W. (1997) Mass spectrometric quantification of 3-chlorotyrosine in human tissues with attamole sensitivity: A sensitive and specific marker for myeloperoxidase-catalysed chlorination at sites of inflammation, *Free Radical Biol. Med. 23*, 909−916.
40. Fu, S., Wang, H., Davies, M. J., and Dean, R. T. (2000) Reaction of hypochlorous acid with tyrosine and peptidyl-tyrosyl residues gives dichlorinated and aldehydic products in addition to 3-chlorotyrosine, *J. Biol. Chem. 275*, 10851−10857.
41. Domigan, N. M., Charlton, T. S., Duncan, M. W., Winterbourn, C. C., and Kettle, A. J. (1995) Chlorination of tyrosyl residues in peptides by myeloperoxidase and human neutrophils, *J. Biol. Chem. 270*, 16542−16548.
42. Winterbourn, C. C., and Kettle, A. J. (2000) Biomarkers of myeloperoxidase-derived hypochlorous acid, *Free Radical Biol. Med. 29*, 403−409.
43. Gaut, J. P., Byun, J., Tran, H. D., and Heinecke, J. W. (2002) Artifact-free quantification of free 3-chlorotyrosine, 3-bromtyrosine, and 3-nitrotyrosine in human plasma by electron capture-negative chemical ionization gas chromatography mass spectrometry and liquid chromatography-electrospray ionization tandem mass spectrometry, *Anal. Biochem. 300*, 252−259.
44. Gaut, J. P., Yeh, G. C., Tran, H. D., Byun, J., Henderson, J. P., Richter, G. M., Brennan, M. L., Lusis, A. J., Belaaouaj, A., Hotchkiss, R. S., and Heinecke, J. W. (2001) Neutrophils employ the myeloperoxidase system to generate antimicrobial brominating and chlorinating oxidants during sepsis, *Proc. Natl. Acad. Sci. U.S.A. 98*, 11961−11966.
45. Kelly, F. J., and Mudway, I. S. (2003) Protein oxidation at the air-lung interface, *Amino Acids 25*, 375−396.
46. Lamb, N. J., Gutteridge, J. M. C., Baker, C., Evans, T. W., and Quinlan, G. J. (1999) Oxidative damage to proteins of bronchoalveolar lavage fluid in patients with acute respiratory distress syndrome: Evidence for neutrophil-mediated hydroxylation, nitration and chlorination, *Crit. Care Med. 27*, 1738−1744.
47. Armesto, X. L., Canle, L., and Santaballa, J. A. (1993) α-Amino acids chlorination in aqueous media, *Tetrahedron 49*, 275−284.
48. Antelo, J. M., Arce, F., and Parajo, M. (1995) Kinetic study of the formation of *N*-chloramines, *Int. J. Chem. Kinet. 27*, 637−647.
49. Prutz, W. A. (1998) Interactions of hypochlorous acid with pyrimidine nucleotides, and secondary reactions of chlorinated pyrimidines with GSH, NADH, and other substrates, *Arch. Biochem. Biophys. 349*, 183−191.
50. Hawkins, C. L., Pattison, D. I., and Davies, M. J. (2002) Reaction of protein chloramines with DNA and nucleosides: Evidence for the formation of radicals, protein-DNA cross-links and DNA fragmentation, *Biochem. J. 365*, 605−615.
51. Vissers, M. C., Carr, A. C., and Chapman, A. L. (1998) Comparison of human red cell lysis by hypochlorous and hypobromous acids: Insights into the mechanism of lysis, *Biochem. J. 330*, 131−138.
52. Hawkins, C. L., Brown, B. E., and Davies, M. J. (2001) Hypochlorite- and hypobromite mediated radical formation and its role in cell lysis, *Arch. Biochem. Biophys. 395*, 137−145.
53. Morris, J. C. (1966) The acid ionization constant of HOCl from 5 °C to 35 °C, *J. Phys. Chem. 70*, 3798−3805.
54. Margerum, D. W., and Huff Hartz, K. E. (2002) Role of halogen(I) cation-transfer mechanisms in water chlorination in the presence of bromide ion, *J. Environ. Monit. 4*, 20−26.
55. Eigen, M., and Kustin, K. (1962) The kinetics of halogen hydrolysis, *J. Am. Chem. Soc. 84*, 1355−1361.
56. Lentner, C., Ed. (1984), *Geigy Scientific Tables: Physical Chemistry, Composition of Blood, Hematology, Somatometric Data*, Vol. 3, Ciba-Geigy, Basle.
57. Wasil, M., Halliwell, B., Hutchison, D. C. S., and Baum, H. (1987) The antioxidant action of human extracellular fluids, *Biochem. J. 243*, 219−223.
58. Hu, M. L., Louie, S., Cross, C. E., Motchnik, P., and Halliwell, B. (1993) Antioxidant protection against hypochlorous acid in human plasma, *J. Lab. Clin. Med. 121*, 257−262.
59. Halliwell, B. (1988) Albumin—an important extracellular antioxidant, *Biochem. Pharmacol. 37*, 569−571.
60. Gallard, H., and von Gunten, U. (2002) Chlorination of phenols: Kinetics and formation of chloroform, *Environ. Sci. Technol. 36*, 884−890.
61. Gallard, H., Pellizzari, F., Croue, J. P., and Legube, B. (2003) Rate constants of reactions of bromine with phenols in aqueous solution, *Water Res. 37*, 2883−2892.
62. van Dalen, C. J., Whitehouse, M. W., Winterbourn, C. C., and Kettle, A. J. (1997) Thiocyanate and chloride as competing substrates for myeloperoxidase, *Biochem. J. 327*, 487−492.
63. Carr, A. C., Decker, E. A., Park, Y., and Frei, B. (2001) Comparison of low-density lipoprotein modification by myeloperoxidase-derived hypochlorous and hypobromous acids, *Free Radical Biol. Med. 31*, 62−72.
64. Dallegri, F., Patrone, F., Ballestrero, A., Frumento, G., and Sacchetti, C. (1986) Inhibition of neutrophil cytolysin production by target cells, *Blood 67*, 1265−1272.
65. Vissers, M. C., Stern, A., Kuypers, F., van den Berg, J. J. M., and Winterbourn, C. C. (1994) Membrane changes associated with lysis of red blood cells by hypochlorous acid, *Free Radical Biol. Med. 16*, 703−712.
66. Vissers, M. C., and Winterbourn, C. C. (1995) Oxidation of intracellular glutathione after exposure of human red blood cells to hypochlorous acid, *Biochem. J. 307*, 57−62.

BI035946A